Instant Release Fraction Corrosion Studies of Commercial UO_2 BWR Spent Nuclear Fuel

Albert Martínez-Torrents[1*], Daniel Serrano-Purroy[2], Rosa Sureda[1], Ignasi Casas[3], Joan de Pablo[1,3]

[1] *Fundació CTM Centre Tecnològic, Plaça de la Ciència 2, 08243 Manresa, Spain*

[2] *European Commission, DG Joint Research Centre - JRC, Directorate G - Nuclear Safety & Security, Department G.III, P.O. Box 2340, D-76125 Karlsruhe, Germany*

[3] *Department of Chemical Engineering, Universitat Politècnica de Catalunya – Barcelona Tech, Eduard Maristany 14, 08019 Barcelona , Spain.*

** Corresponding author: albert.martinez@ctm.com.es*

Abstract

The instant release fraction of a spent nuclear fuel is a matter of concern in the performance assessment of a deep geological repository since it increases the radiological risk. Corrosion studies of two different spent nuclear fuels were performed using bicarbonate water under oxidizing conditions to study their instant release fraction. From each fuel, cladded segments and powder samples obtained at different radial positions were used. The results were normalised using the specific surface area to permit a comparison between fuels and samples.

Different radionuclide dissolution patterns were studied in terms of water contact availability and radial distribution in the spent nuclear fuel.

The relationship between the results of this work and morphological parameters like the grain size or irradiation parameters such as the burn-up or the linear power density was studied in order to increase the understanding of the instant release fraction formation.

1. Introduction

Performance Assessment (PA) studies of spent nuclear fuel (SNF) storage considers several barriers to prevent the contact of the SNF with the groundwater and the following release of radionuclides (RN) into the environment. The Spent Fuel Matrix itself is considered as a barrier for the RN release. During the fuel irradiation some of the fission products generated are segregated from the matrix and diffuse according to temperature gradients in the fuel during in-pile operation accumulating in the void spaces: gap between fuel and cladding, fractures, bubbles and grain boundaries. This re-distribution depends on the characteristics of the irradiation: the linear power density (LPD), the irradiation history and the burn-up (BU). The grain size affects also the re-distribution of segregated fission products. The size of the grain determines the time required for the RN to reach the grain boundary, being higher for bigger grains. Therefore, the industry is trying to create fuels with larger grains to decrease the release of RN, especially fission gases, and thus being able to reach higher burn-ups, obtaining more energy per gram of fuel.

The matrix of the fuel will keep most of the RN inside and they will be released only as a function of the matrix dissolution. This dissolution will vary depending on the groundwater composition and the RedOx characteristics. Also the RN release will vary as a function of their chemical state, their distribution and their solubility. Nevertheless it is considered that those RN that are not trapped in the matrix due to the segregation during the irradiation will not be released congruently with the matrix. Depending on water accessibility, the segregated RN will be released into the environment in a short period of time covering days to months. This fraction of RN that dissolves faster than the matrix, is known as Instant Release Fraction (IRF) or Fast Release Fraction (FRF). The PA considers the IRF to be one of the main sources of radiological risk in geological disposal [1].

Nuclear power-plants are increasing the burn-up of the fuel in order to take the maximum energy of each rod increasing the efficiency. At burn-ups higher than 40 $MWd(KgU)^{-1}$, the neutron capture of ^{238}U to produce ^{239}Pu, creates an external layer on the fuel with a higher burn-up, higher porosity and fuel grain subdivision. This external layer is known as the High Burn-up Structure (HBS)[2-7] or Rim.

There is a lack of data in the field of the IRF processes, especially for High Burn-up (HBU) fuels. Our group is working in order to increase the knowledge on this field and has published several works on this topic in the recent years [1,7-10]. Also in the last three years a collaborative project known as FIRST NUCLIDES PROJECT [11] has focused the effort of several universities, research centres and institutions in the improvement of the understanding of the IRF.

In the present work the IRF of two different BWR (Boiling Water Reactor) fuels with different burn-up (42 and 54 $MWd(KgU)^{-1}$) and well known irradiation histories were studied through different

corrosion tests. Leaching tests were performed using both cladded pieces and powdered fractions of fuel. In order to study the effect of the HBS in the IRF, two different powder fractions were used for each SNF. One was obtained from the centre of the pellet (CORE) and the other was obtained from the periphery of the pellet (OUT), enriched in HBS.

2. Experimental

2.1. Irradiation parameters

Two SNF UO_2 rods irradiated in different commercial BWRs were selected for the leaching experiments. In this document, samples were named according to the average burn-up of the original SNF rods. The SNF with an average burn-up of 42 $MWd(kgU)^{-1}$ and 54 $MWd(kgU)^{-1}$ are referred as 42BWR and 54BWR respectively. The local burn-up of the samples used was determined for each fuel, being 45 $MWd(kgU)^{-1}$ for the 42BWR and 58 $MWd(kgU)^{-1}$ for the 54BWR. The 42BWR rod was irradiated with an average linear power density of 217 Wcm^{-1} and a maximum linear power density of 293 Wcm^{-1}. The available irradiation data for the 54WR were more precise, and in this case the linear power of the rod but also the linear power for the position of the samples used in this work was known. The average linear power for the position of the samples used in this work was 165 Wcm^{-1} and the maximum linear power during the irradiation was 275 Wcm^{-1}. The fuel enrichment was 3.7% ^{235}U and 4.2% ^{235}U for 42BWR and 54BWR respectively. The fission gas release was 2.3±0.2% for the 42BWR and 3.9±0.4% for the 54BWR. The effect of these irradiation parameters is taken into account in the discussion of the inventory and corrosion studies.

2.2. Sample preparation

The IRF of a UO_2 fuel was studied using cladded segments and powder fractions. The cladded segment experiments allowed the determination of the contribution of the RN trapped in the gap between the cladding and the pellet, the cracks and the fractures to the total IRF. Similarly, the powder fraction experiments were used to study the contribution coming from the grain boundaries to the total IRF. The RN are not homogenously distributed in the fuel pellet due to the segregation during the irradiation. Therefore, powder fractions from the centre and the periphery of the fuel were used to study the effect of the radial heterogeneity of the fuel in the IRF release. In addition the effect of the HBS in the periphery of the fuel pellet was also taken into account.

2.2.1. Cladded segments

Gamma scanning was used to determine the most homogeneous regions with the highest burn-up in the selected rods. Then an initial longitudinal cut of approximately 20 mm was performed along the segments to determine pellet boundaries, see Figure 1. The inter-pellet zones or dishing are ususally rich in IRF RN such as Cs but the contribution of this fraction to the total IRF is not known. In order to simplify the discussion of the results this zone was purposely avoided during the cut of the segments.

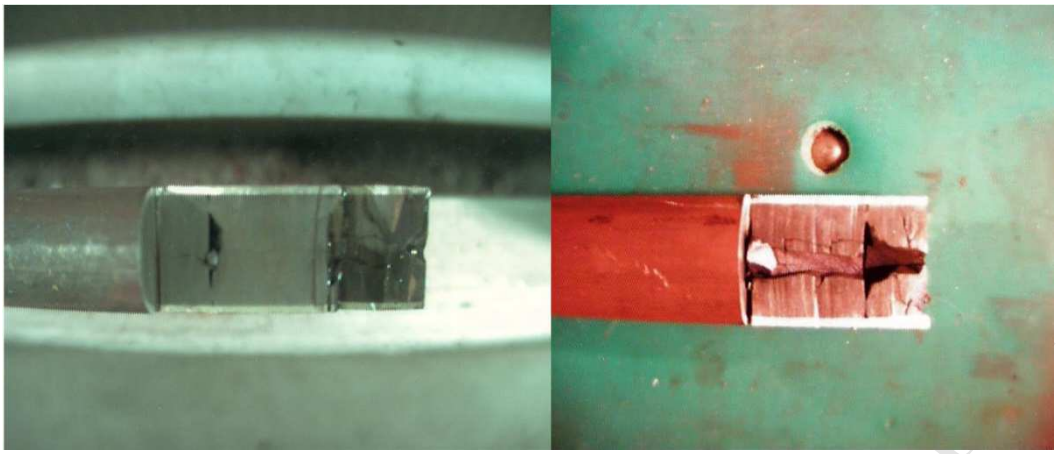

Figure 1. *Longitudinal cut section to determine pellet boundaries in the 54BWR and the 42BWR fuel.*

In both cases, another cladded segment next to the one used for the experiment was cut, also avoiding inter-pellet boundaries, in order to use it for the chemical inventory determination.

The characteristics of the cladded segments are shown in Table 1.

Table 1. SNF samples selected for the cladded segment experiments

Cladded Segment	**42BWR**	**54BWR**
Length (mm)	2.8±0.1	2.5±0.1
Diameter without cladding (mm)	9.4±0.1	8.7±0.1
Segment weight with cladding (g)	2.3614±0.0001	2.0617±0.0001
Segment weight without cladding (g)[a]	1.79±0.05	1.64±0.05
Surface area (mm^2)[b]	500±10	420±10
S/V (mm^{-1})	10±1	9±1
Grain size (µm)	15.0±1.0	10.1±1.0
FGR (%)	2.3	3.9
Local burn-up ($GWd(t_{HM})^{-1}$)[c]	45	58
Av. Linear Power density (W/cm)	217	165
Irradiation time (days)	1475	1820

a. The weight of the pellet without cladding was estimated from the ratio pellet to cladding obtained after complete dissolution of a pellet for inventory determination.

b. The surface area exposed was calculated taking into account the total surface in contact with solution (both faces of the slice) and a roughness factor of 3.5 [12].

c. Estimated from gamma scanning and cutting plan positions.

In Figure 2 an image of the cross sections of the sample 54BWR is shown. Fractures caused by the high thermal gradients during the irradiation are common in the fuel pellets and these samples are not an exception.

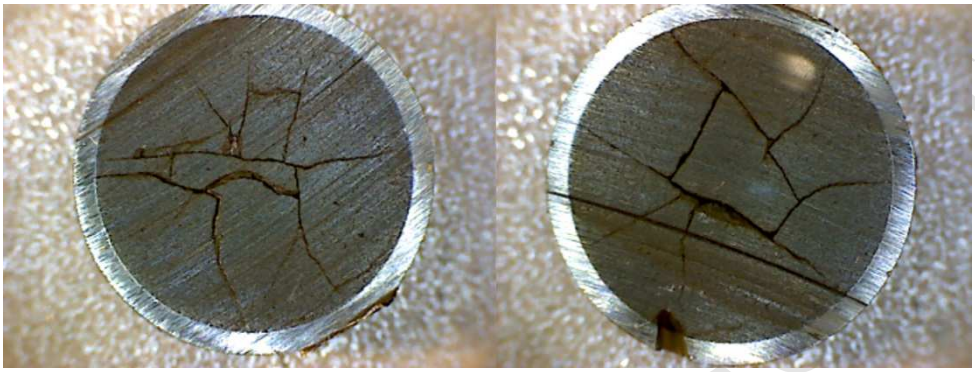

Figure 2. *Cross sections of 54BWR spent fuel sample used in the leaching experiment.*

2.2.2. Powder samples

The powder samples were obtained from the centre (CORE) and the periphery of the pellet (OUT) using the following procedure:

1. Cutting: A piece of approximately 3-4 cm was cut from the selected segment (Figure 3).

2. Drilling: Powder samples from the CORE region of the pellet were obtained drilling at the centre of the segment with a drill bit of 3mm (Figure 4). Then, a fraction not used in this work was collected using a bit of 8 mm. Finally, the OUT fraction was obtained from the remaining fuel attached in the walls of the cladding. It was obtained by pressuring the cladding to release the fuel fraction.

3. Milling and sieving: Powder samples were milled (M20 KA, IKA Gmbh, Germany) and sieved (Vibrax-VXR, IKA Gmbh, Germany) in order to obtain fractions of powder with different particle sizes. In the experiments presented in this work particles with a particle size between 50 and 100 µm were used.

4. SEM characterisation: Scanning Electron Microscopy (SEM)(JEOL 6400, JEOL ltd, Japan) was used in order to know the average diameter size of the particles used in the experiments (Figure 5).

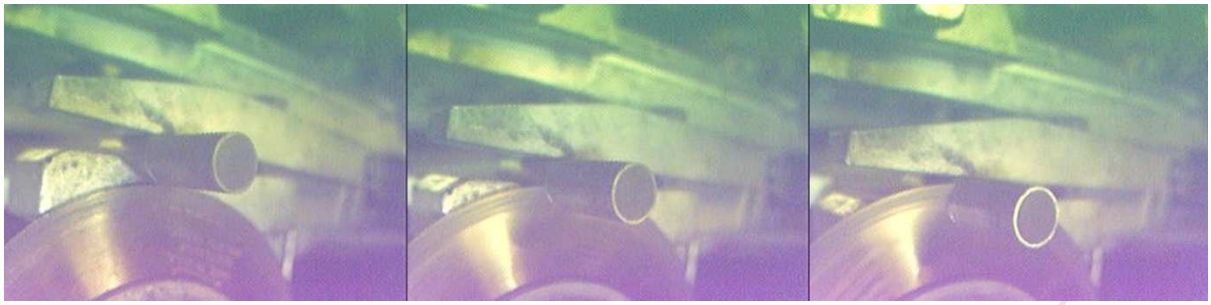

Figure 3. *Cutting of cladded segments for 54BWR fuel samples.*

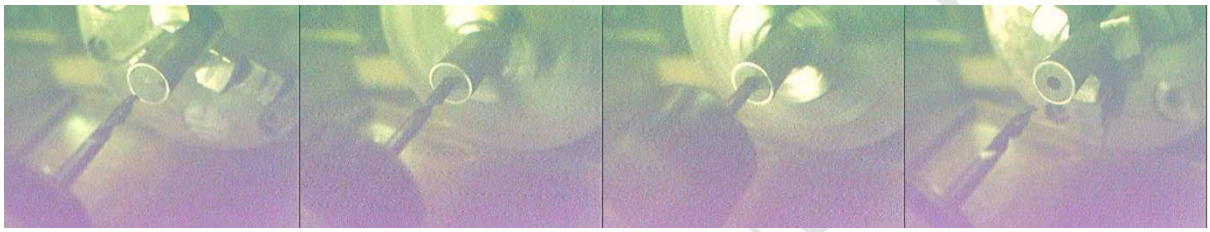

Figure 4. *Drilling of cladded segments for 54BWR fuel samples.*

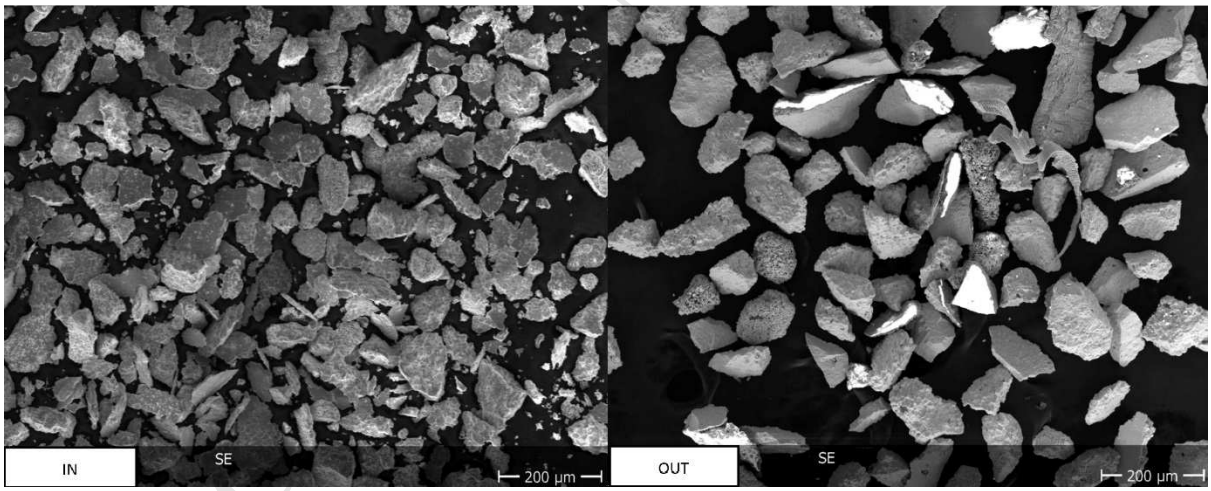

Figure 5. *Powder particles of 54BWR fuel samples.*

The characteristics of the powder used are found in Table 2.

Table 2. SNF samples selected for the powder experiments.

Powder	42BWR CORE	42BWR OUT	54BWR CORE	54BWR OUT
Powder sample weight (g)	0.1089±0.0001	0.1167±0.0001	0.1386±0.0001	0.0902±0.0001
Powder particle size (µm)[a]	50±20	46±20	73±28	91±37
Fuel density (g/cm^3)	10.53±0.01	10.53±0.01	10.45±0.01	10.45±0.01
Surface area (mm^2)[b]	4420±3000	5110±4000	3840±1750	2000±970
S/V (m^{-1})	90±60	100±80	75±35	40±20

a. The mean particle size was measured following the same procedure as in [1].

b. Specific surfaces area were estimated for each SNF fraction assuming a spherical shape of the particles and a roughness factor of 3.5 [12].

2.3. Experimental set-up

The leachate used in the experiments was a carbonated solution (1mM $NaHCO_3$ + 19mM NaCl), with initial pH of (8.4 ± 0.1) that was initially equilibrated with air under oxidizing conditions and a normal hot cell temperature (25 ± 5)°C. For all experiments a volume solution of (50 ± 1) cm^3 was used.

The cladded segments were suspended into a plastic vessel through a platinum thread (Figure 6). A stirrer was used to keep the vessel under continuous orbital rotation. Homogenization of the solution and full contact within sample and leaching solution is ensured by the system at all contact times. To avoid the loss of valuable information concerning the IRF, no previous washing steps were performed in cladded segment samples.

Figure 6. *Experimental set-up.*

Vessels filled only with the carbonated solution were used as blank tests using the same procedure.

The contact periods were: 0.1, 0.2, 1, 4, 8, 21, 49, 83, 162 and 190 days. After each one, the whole solution was renewed.

Powdered samples leaching tests were prepared adding a known quantity of the selected fuel powder to a glass tube and then (50 ± 1) cm^3 of the sample-leaching solution were added. The glass tubes were continuously stirred. In this case the hot cell blanks were two tubes with the same solution but without fuel powder. Although some IRF contribution might be lost, the high amount of fines present in the powder samples as a consequence of the sample preparation, justified a prewashing step. After that, the solution was renewed at each sampling. The contact periods were 0.8, 2, 3, 4, 7, 9, 11, 16, 22, 30, 81 and 116 days.

In all cases, unfiltered aliquots of fuel solutions were diluted and acidified with 1 M HNO_3.

ICP-MS analyses were performed using a Thermo ELEMENT 2 instrument (Thermo Electron Corporation, Germany). Calibration curves were produced using a series of dilutions of certified multi-element standard solutions in the concentration range of the major elements in solution. Co, In, Ho and Th were used as internal standards in the sample measurements. The concentrations of the elements were calculated from the isotopic data. Whenever was possible, isobaric interferences were corrected based on isotopic ratios previously calculated with the ORIGEN code (ORIGEN-ARP, 2000) as a reference.

Measurements of pH were performed during the entire experiment using an Orion 525A+ pH-meter, a gel pH Triode L/M (reference 9107BN) supplied from Thermo-Electron, USA. The pH electrode was calibrated with commercial pH buffer solutions (METLER TOLEDO Inc., USA; pH 4.01 (Ref.501307069), pH 7.00 (Ref.51302047), pH 9.21 (Ref.51302070)).

2.4. Inventory determination.

The theoretical inventory was calculated using the ORIGEN code (ORIGEN-ARP, 2000).

For each fuel the inventory was experimentally determined using a cladded segment, and also using powder from the centre (CORE) and from the periphery of the pellet (OUT). The experimental determination was performed using ICP-MS and γ-spectrometry.

Cladded segment inventory determination experiments were carried out by dissolving the fuel (1.157g for the 42BWR fuel and 1.425g for the 54BWR fuel) in 250 ml of 8 mol dm^{-3} HNO_3. The experiments were carried during 5 hours at 110-135 °C. After the heating the solution was filtered in order to remove the cladding and insoluble materials.

To determine experimentally the powder inventories, approximately 0.05 g of powder were dissolved in acid using a Parr Teflon bomb. Each powder was dissolved in two different acidic media: in 30 ml of 0.1 mol dm^{-3} HF in concentrated HNO_3 solution at 210°C and in 30ml of a mixture HNO_3:HCl (180:70 volume ratio) at 180°C to correct for lanthanide fluoride precipitation. Both dissolution experiments lasted 12 hours. After the experiments no solid parts were observed.

Dilutions 1/10000 and 1/100000 were analysed using ICP-MS. The last dilution was analysed by γ-spectrometry as well.

2.5. Data treatment

The total released or cumulative moles in solution for element *i*, *cummoles(i)*, is calculated considering the total amount of radionuclide *i* removed in each sampling:

$$\mathrm{cummoles}(i) = \sum_{0}^{n} \mathrm{moles}_{\mathrm{sample}}\,(\mathrm{n},\mathrm{i}) \qquad (1)$$

where $moles_{sample}\,(n,i)$ correspond to the moles in solution before each complete replenishment *n*.

The cumulative concentration $cumC_i$ of an element *i* in moles·dm^{-3} is then calculated as:

$$\mathrm{cumC_i} = \frac{\mathrm{cummoles\ (i)}}{\mathrm{V}} \qquad (2)$$

where *V* corresponds to the average volume of the dissolution samples in dm^{-3}.

The Cumulative Fraction of Inventory of an element *i* released in the Aqueous Phase (Cum$FIAP_i$) is given by Equation 3.

$$CumFIAP_i = \frac{m_{i,aq}}{m_{i,SNF}} = \frac{c_i\, V_{aq}}{m_{SNF}\, H_i} \qquad (3)$$

where $m_{i,aq}$ is the cumulative mass of element *i* in the aqueous phase in g, $m_{i,SNF}$ the mass of element *i* in the SNF sample in g, m_{SNF} the mass of SNF used in the experiment in g, H_i corresponds to the fraction of inventory for the nuclide *i* in g/g, c_i is the cumulative concentration of element *i* in solution in g dm^{-3} and V_{aq} is the volume of solution in dm^3. The CumFIAP has no units but is presented in percentage.

The Cumulative Fractional Release Normalised to Uranium for an element *i* ($CumFNU_i$) is given by Equation 4.

$$CumFNU_i = \frac{CumFIAP_i}{CumFIAP_U} \qquad (4)$$

where $FIAP_i$ and $FIAP_U$ are the FIAP of element *i* and uranium, respectively.

The Instant Release Fraction for an element *i* (IRF_i) is given by Equation 5.

$$IRF_i = cumFIAP_i - \mathrm{cum}FIAP_U \quad (5)$$

Finally, the Instant Release Fraction for an element *i* normalised to the specific surface area (IRFS_i) is:

$$IRFS_i = \frac{IRF_i}{S} \quad (6)$$

where *S* is the specific surface area (m^2g^{-1}). The specific surface area was calculated in each case dividing the total surface area (m^2) by the mass of the sample (g). The IRF is presented in percentage and the IRFS in percentage per g m^{-2}.

3. Results

3.1. pH evolution

Initially the pH of the solutions was in average 8.4±0.1 and decreased down to 7.6±0.1 at the end of the experiments, possibly due to the uranium oxide surface buffer capacity [13].

3.2. Inventory results

The experimental inventory results are given in Tables 3 and 4. Calculated (KORIGEN) inventories are also given for comparison.

Table 3: Radionuclide inventory for 42BWR fuel.

Element	CORE (µg /g fuel)	OUT (µg /g fuel)	Segment (µg /g fuel)	Calculated (µg /g fuel)
Rb	400±60	400±40	400±50	400
Sr	1100±80	1200±100	800±80	800
Y	500±70	700±90	500±100	500
Zr	4500±300	5700±300	4700±300	4200
Mo	3800±300	4800±400	3600±500	3800
Tc	800±100	1100±100	800±100	900
Ru	2400±200	3000±300	1700±300	2300
Rh	500±50	700±90	300±60	500
Pd	1400±300	2600±400	2300±500	1600
Cs	2800±200	3300±300	2600±300	2700
Ba	7700±500	4300±300	2100±1800	2100
La	1500±100	1900±200	1500±200	1400
Ce	2700±200	3400±300	2700±300	2700
Pr	1300±100	1800±200	1300±200	1300
Nd	5500±600	6900±800	5500±1000	4400
Sm	1000±300	1200±200	1200±400	1000
U	844500±25000	826500±18000	823800±24000	833500
Np	600±100	900±100	600±100	500
Pu	10500±700	13000±1000	10800±1000	8700
Am	200±40	500±90	300±90	800
Cm	40±20	100±50	100±40	30

According to Table 3, in the case of the 42BWR spent nuclear fuel, the experimental inventory of the cladded segment is not significantly different to the calculated values. However, both powder fractions present significant differences. In the periphery of the fuel (OUT sample) the uranium

content is lower, whereas the minor actinides (MAn) and the fission products (FP) are more abundant than the calculated values. On the contrary, in the centre of the fuel (CORE sample) the results are the opposite, more uranium and less MAn and FP content than the calculated values are found.

Experimental core to out ratios can be explained in terms of local differences in burnup, where non-mobile elements like Nd follow the sample burnup radial profile, as well as in terms of segregation and redistribution during irradiation according to temperature profiles, where mobile elements like Cs accumulate in the periphery of the fuel.

Table 4: Radionuclide inventory for 54BWR fuel.

Element	CORE (µg /g fuel)	OUT (µg /g fuel)	Segment (µg /g fuel)	Calculated (µg /g fuel)
Rb	400±80	500±100	500±80	500
Sr	1200±670	1400±770	1300±700	1100
Y	600±110	700±140	700±140	600
Zr	4800±900	7100±1400	6100±1200	5200
Mo	4100±1100	7300±1900	4700±1300	4800
Tc	900±200	1300±200	1000±200	1100
Ru	2700±500	4000±800	2600±500	3100
Rh	500±120	800±190	600±150	600
Pd	1600±700	1300±500	3500±1300	2200
Cs	3200±500	4400±700	3900±600	3700
Ba	5400±1400	4800±1200	3700±1000	2600
La	1600±300	2400±500	2200±400	1800
Ce	2900±600	4300±800	3600±700	3500
Pr	1500±300	2200±400	2000±400	1600
Nd	5900±1100	8800±1600	7300±1300	5600
Sm	1500±300	2300±500	2100±500	1200
U	817000±53000	831500±54000	909800±47000	822400
Np	1000±100	1200±200	1300±200	600
Pu	9300±1600	13200±2300	11500±2100	8900
Am	100±40	200±100	200±70	600
Cm	100±40	200±90	100±60	100

Similar conclusions can be drawn from Table 4. The inventory of fission products in the 54BWR fuel is moderately higher due to its higher burn-up. Anyhow, the uranium inventory of the 54BWR cladded segment is significantly higher than the calculated and the powder values The higher uncertainty of the experimental data originates most probably from the hotcell sample

manipulation. However, the chemical elemental ratio is not significantly different from the ratio in the calculated inventory.

These experimental inventory values were used to calculate the Fraction of Inventory in the Aqueous Phase (FIAP) in the following sections, with one exception: sample 54BWR cladded segment, where the calculated inventory was used to avoid underestimation of the released fractions.

3.3. Radionuclide moles in solution

In this work only some representative radionuclides will be shown: Rb, Sr, Mo, Tc, Cs and U. They were selected based on the experience of previous works [1,7-8].

If no secondary phase is formed, U is a good matrix indicator and can be used to determine the evolution of the matrix in the experiments. In the reported experiments, Uranium speciation studies performed at each contact period confirmed that secondary phases (mainly Schoepite) saturation limits were not reached. Rb, Sr, Mo, Tc and Cs were selected as typical IRF RN.

In Figure 7 the cumulative moles in solution of the cladded segment of the 42BWR fuel are represented as a function of the cumulative leaching time as an example of the evolution of the different elements with time. The evolution in all the experiments performed was very similar, an initial fast dissolution followed by a slower second contribution.

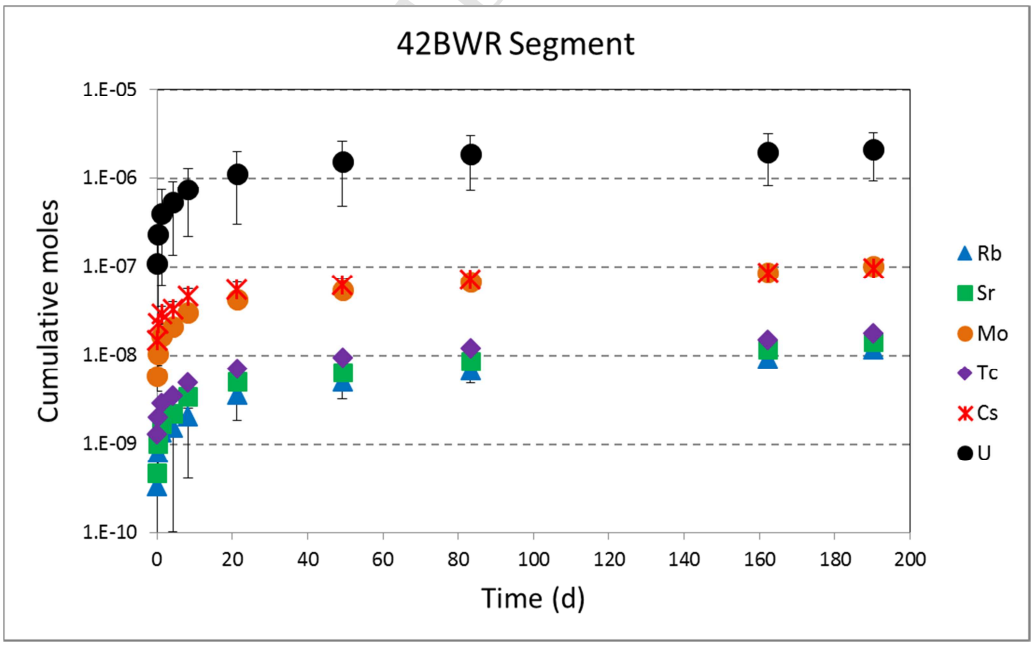

Figure 7: *Elemental cumulative moles vs time. Experiment carried out with the 42BWR cladded segment.*

Although at first sight all the elements studied seemed to have a similar behaviour, it is necessary to normalise the results by the inventory of each element to compare them correctly.

4. Discussion

4.1 Fraction of Inventory in the Aqueous Phase (%) and Fraction release Normalised to Uranium.

In addition to cumulative moles, and taking into account the experimental inventory, cumulative FIAP (Fraction of Inventory in Aqueous Phase) values were also calculated, see Figures 8 to 13. For the 54BWR Segment experiment the calculated inventory was used instead of the experimental inventory, due to the uncertainties coming from the inherent operational complexity of working in the hot cells.

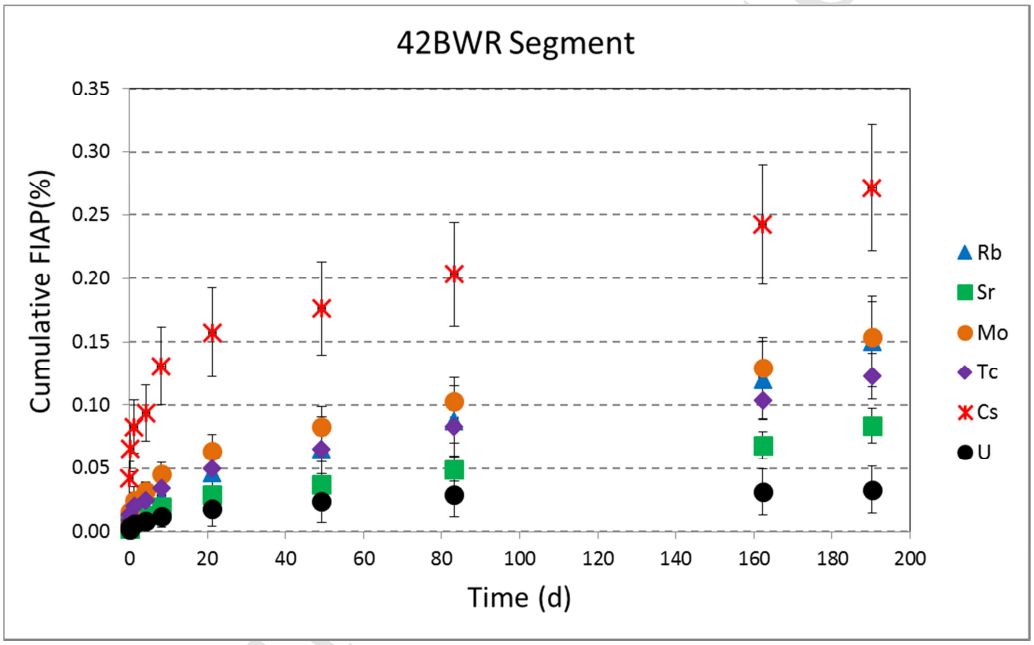

Figure 8: *Cumulative FIAP(%) vs time. Experiment carried out with the segment of the 42BWR fuel.*

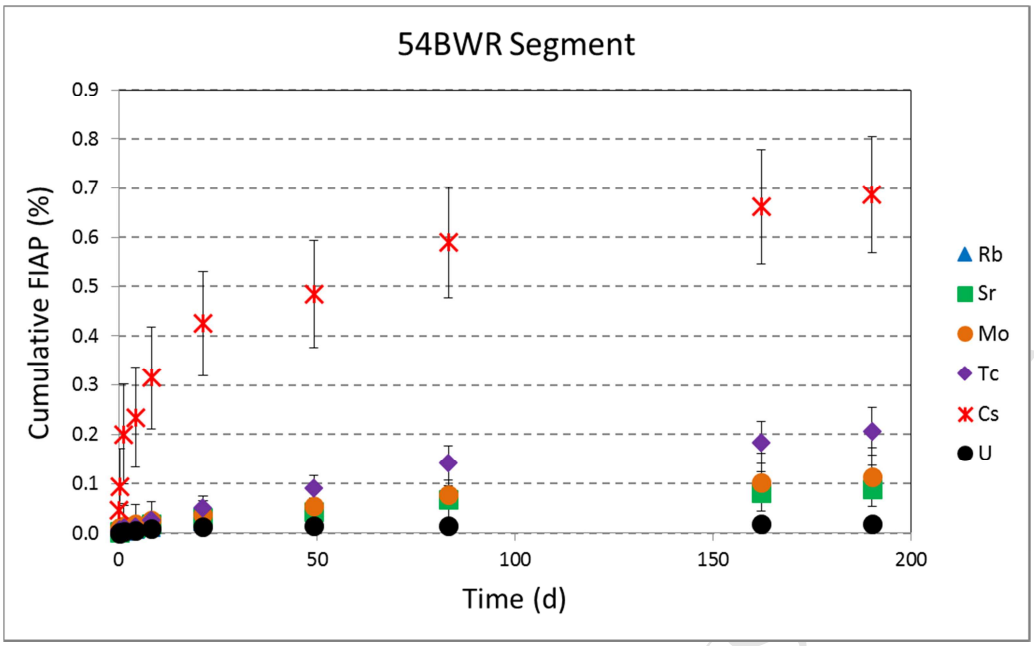

Figure 9: *Cumulative FIAP(%) vs time. Experiment carried out with the segment of the 54BWR fuel.*

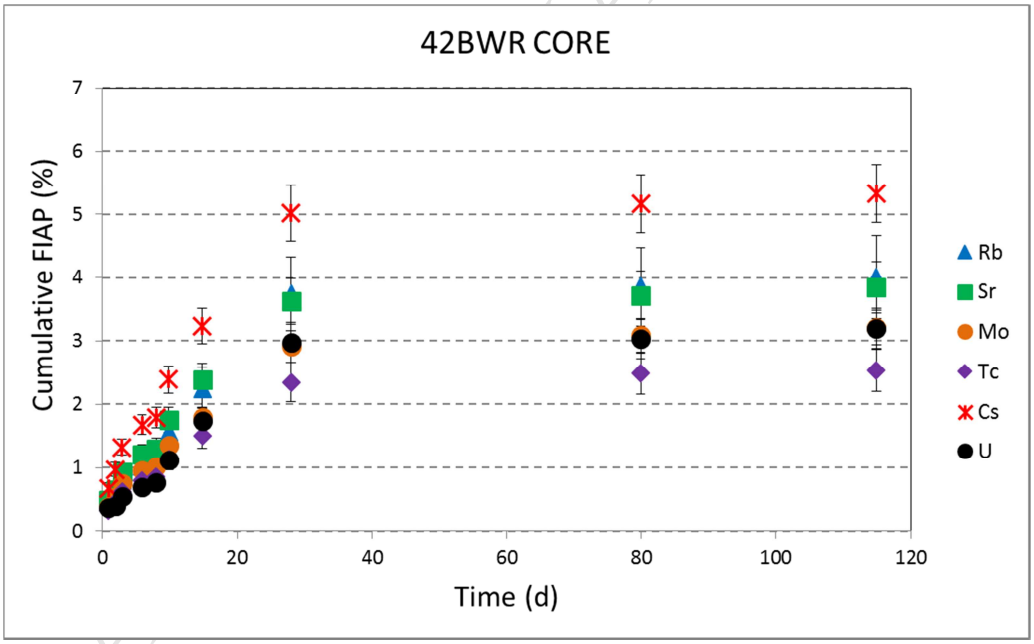

Figure 10: *Cumulative FIAP(%) vs time. Experiment carried out with powder from the centre (CORE) of the 42BWR SNF.*

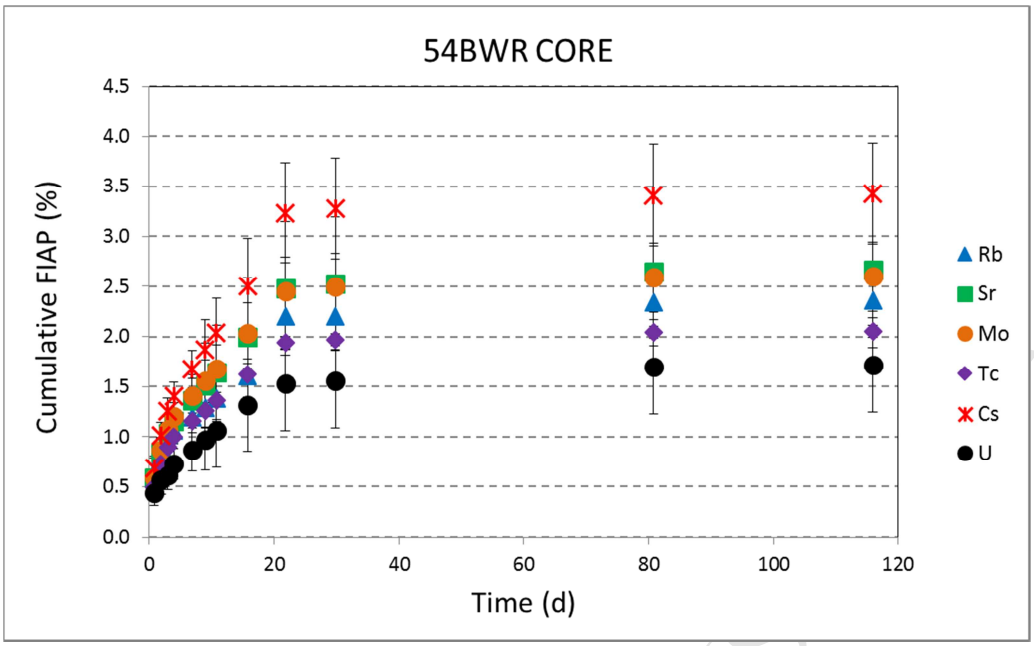

Figure 11: *Cumulative FIAP(%) vs time. Experiment carried out with powder from the centre (CORE) of the 54BWR SNF.*

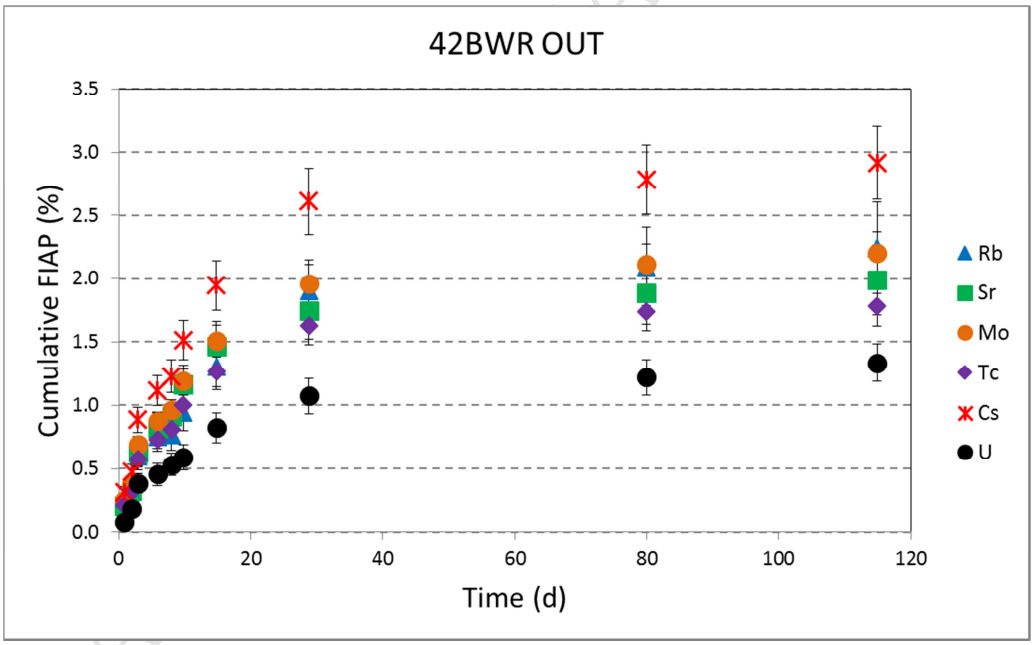

Figure 12: *Cumulative FIAP(%) vs time. Experiment carried out with powder from the periphery (OUT) of the 42BWR SNF.*

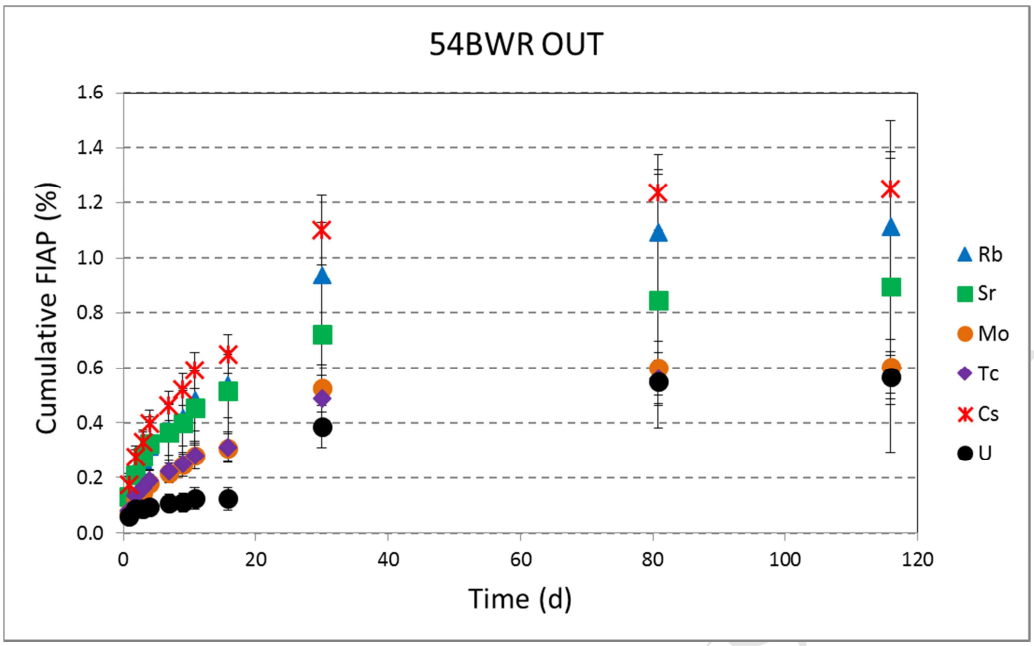

Figure 13: *Cumulative FIAP(%) vs time. Experiment carried out with powder from the periphery (OUT) of the 54BWR SNF.*

The radionuclides generated during the irradiation can be redistributed along the fuel depending on their melting and boiling point. This redistribution is driven by the temperature gradient produced by the difference in the temperature of the center and the temperature of the periphery of the fuel pellet that is closer to the coolant. On the spent fuel the elements that have been segregated during irradiation will be found in the gap between the cladding and the pellet, in the cracks, in the fractures and in the grain boundaries. The reactivity and oxidation state of the new radionuclides will also affect the speciation and the new elements will be found in different phases such as metallic phases, oxides or forming ε-particles. These phenomena produce a different dissolution rate depending on the element and its phase, that has been already observed in previous works [1,7-8]. Some radionuclides dissolve with the uranium matrix, but some others dissolve faster or even slower.

The two different trends previously observed in figure 7 are more easily spotted now in these cumulative FIAP figures. The dissolution rate of the radionuclides studied in this work decreased with the experimental time . This decrease has different explanations depending on the kind of radionuclide. The faster dissolution at the beginning for the radionuclides that dissolve at the same rate or slower than the matrix could be due to the dissolution of preoxidized layers and fines. On the other hand, in the case of the radionuclides that dissolve faster than the matrix, the fraction immediately available in the gap, cracks and grain boundaries was quickly released after the contact with the solution, producing an initial dissolution rate faster than the rate of the following days.

After the initial days the dissolution rate depended on the time that the solution needed to reach the internal grain boundaries, releasing the radionuclides trapped there.

In all the experiments Cs was the element with the highest FIAP. Oppositely uranium was the element with the lowest FIAP in all the cases except for the 42BWR CORE experiment. In this experiment Mo and Tc present a release similar to U. The elements Rb, Sr, Mo and Tc tended to follow the same trend with FIAPs between the FIAP of the Cs and the FIAP of U. None of the FIAPs of these 4 elements outstood among the others. Differences from one experiment to another could be due to differences in the speciation of the elements in the fuel or simply due to random effects. In any case, with the exception of the 42BWR CORE experiment, all these radionuclides dissolved faster than uranium.

Comparing the cumulative FIAP values between powder fractions and cladded segment, differences up to 2 orders of magnitude were found for uranium FIAP values, higher in the powder fraction experiments. One explanation could be that, although it was made at low speed, the drilling and milling of the powder samples caused heating and oxidation, forming a preoxidased layer of uranium responsible of this initial fast release. However this higher release could also be explained as an artefact produced by the difference in the specific surface between powder fractions and cladded segments. In addition, in the experiments with powder, the prewashing step carried out to remove fines could also have removed part of the uranium preoxidised layer. The cumulative FIAP of uranium at the end of the experiment corrected by the specific surface was calculated and it was: 118(%)gm^{-2} and 86(%)gm^{-2} for the cladded segments and: 79(%)gm^{-2},31(%)gm^{-2},62(%)gm^{-2} and 26(%)gm^{-2} for the powder samples. Although it is possible that the powder sample preparation increased the oxidation of the samples, it is difficult that the difference observed between uranium FIAPs originates only from this oxidation, therefore, it was decided to take into account the difference in specific surface between powder and segment, despite the uncertainty of the surface area.

Using the release of uranium as a reference for the release of the matrix, it is possible to calculate the fraction of an element that is released faster than the matrix using the Cumulative Fraction release Normalised to Uranium (CumFNU). A CumFNU higher than 1 indicates that the radionuclides were segregated from the matrix and therefore belong to the IRF. As can be seen in Tables 5 to 10 the radionuclides had a CumFNU higher than 1, except in the case of the 42BWR CORE experiment, where Mo and Tc had a CumFNU equal and lower than 1. Like it was seen in the cumulative FIAP figures, Cs had the biggest CumFNU. Also after 100 days it is possible to see how the CumFNU decreased with time, suggesting that with enough time the IRF will be completely released and the radionuclides will dissolve congruently with the matrix.

Table 5: *CumFNU at each sampling solution versus cumulative sampling time. Experiment carried out with the 42BWR fuel cladded segment.*

Time (d)	0.1	0.2	1	4	8	21	49	83	162	190
Rb	2	3	3	2	2	3	3	3	4	5
Sr	2	2	2	2	2	2	2	2	2	3
Mo	5	4	4	4	4	3	3	3	4	5
Tc	5	4	3	3	3	3	3	3	3	4
Cs	25	18	13	11	11	9	7	7	8	8

Table 6: *CumFNU at each sampling solution versus cumulative sampling time. Experiment carried out with the 54BWR fuel cladded segment.*

Time (d)	0.1	0.2	1	4	8	21	49	83	162	190
Rb	3	2	1	1	1	2	3	5	6	6
Sr	2	3	3	2	2	2	3	4	5	5
Mo	15	9	5	4	3	3	4	5	6	6
Tc	9	7	4	3	3	4	6	9	10	11
Cs	88	76	65	47	37	33	33	37	37	37

Table 7: *CumFNU at each sampling solution versus cumulative sampling time. Experiment carried out with powder from the centre (CORE) of the 42BWR SNF.*

Time (d)	0,8	2	3	6	8	10	15	29	80	115
Rb	1.2	1.5	1.5	1.4	1.5	1.4	1.3	1.3	1.3	1.3
Sr	1.3	1.6	1.7	1.7	1.7	1.6	1.4	1.2	1.2	1.2
Mo	1.1	1.4	1.4	1.4	1.3	1.2	1.0	1.0	1.0	1.0
Tc	0.9	1.2	1.1	1.1	1.1	1.0	0.9	0.8	0.8	0.8
Cs	1.8	2.4	2.4	2.4	2.3	2.1	1.9	1.7	1.7	1.7

Table 8: *CumFNU at each sampling solution versus cumulative sampling time. Experiment carried out with powder from the centre (CORE) of the 54BWR SNF.*

Time (d)	0.8	2	3	4	7	9	16	30	81	116
Rb	1.4	1.5	1.6	1.4	1.4	1.3	1.2	1.4	1.4	1.4
Sr	1.2	1.3	1.5	1.4	1.4	1.4	1.4	1.5	1.5	1.5
Mo	1.3	1.5	1.7	1.6	1.6	1.6	1.5	1.6	1.5	1.5
Tc	1.1	1.3	1.4	1.4	1.3	1.3	1.2	1.3	1.2	1.2
Cs	1.4	1.6	1.8	1.7	1.7	1.7	1.7	1.9	1.8	1.8

Table 9: *CumFNU at each sampling solution versus cumulative sampling time. Experiment carried out with powder from the periphery (OUT) of the 42BWR SNF.*

Time (d)	0.8	2	3	6	8	10	15	29	80	115
Rb	2.6	1.5	1.5	1.7	1.4	1.6	1.6	1.8	1.7	1.7
Sr	2.5	1.8	1.6	1.8	1.7	2.0	1.8	1.6	1.5	1.5
Mo	3.0	2.1	1.8	1.9	1.8	2.0	1.8	1.8	1.7	1.6
Tc	2.5	1.7	1.5	1.6	1.5	1.7	1.5	1.5	1.4	1.3
Cs	3.7	2.6	2.3	2.5	2.3	2.6	2.4	2.4	2.3	2.2

Table 10: *CumFNU at each sampling solution versus cumulative sampling time. Experiment carried out with powder from the periphery (OUT) of the 54BWR SNF.*

Time (d)	0.8	2	3	4	7	16	30	81	116
Rb	2.3	2.6	3.0	3.3	3.4	4.3	2.4	2.0	2.0
Sr	2.0	2.2	2.9	3.2	3.1	3.8	1.7	1.3	1.3
Mo	1.2	1.4	1.7	1.9	2.0	2.5	1.4	1.1	1.1
Tc	1.3	1.6	1.9	2.0	2.1	2.5	1.3	1.0	1.0
Cs	2.6	2.8	3.4	3.8	3.8	4.7	2.6	2.0	1.9

4.2. Instant Release Fraction (%)

The IRF determinations are based on the FIAP results presented. Although initially Mo and Tc were selected to study the IRF, the effect of the RedOx conditions on their speciation, solubility and segregation, interferes in the determination of their IRF contribution, leading in some cases to negative values. Therefore, only Rb, Sr and Cs were selected to study the IRF. The IRF values at the end of the experiments are shown in Table 11.

Table 11: IRF values at the end of the experiments.

IRF (%)	Rb	Sr	Cs
42BWR Segment	0.12±0.04	0.05±0.02	0.24±0.05
42BWR CORE	0.8±0.7	0.6±0.5	2.1±0.6
42BWR OUT	0.9±0.4	0.7±0.3	1.6±0.3
54BWR Segment	0.09±0.06	0.07±0.01	0.67±0.12
54BWR CORE	0.6±0.8	1.0±0.9	1.7±0.7
54BWR OUT	0.5±0.3	0.3±0.6	0.7±0.2

In all the experiments, Cs is the radionuclide with the highest IRF. Since the morphology of the samples is not the same, the comparison between them using the IRF is not completely correct and might lead to erroneous conclusions if a parameter like the specific surface is not contemplated. Looking at Table 11, the release in the powder fractions is much higher than in the cladded segments. But it is not a fair comparison since the surface area of the powder fractions is approximately 10 times higher, and their weight ten times lower. Another example can be observed also in table 11, when comparing the IRF of Cs OUT fractions. It seems that the release in the 42BWR fuel is two times higher but its surface area is also approximately two times higher. In both examples, the differences in the morphology of the sample made difficult to take any conclusion from the IRF results.

The surface area of the sample in contact with the solution is directly proportional to the RN release. In addition, taking into account that the FIAP is the amount of RN in solution divided by the amount of RN in the solid sample, samples of the same fuel with different weight but similar exposed surface will result in different FIAP values, despite having the same release. In order to compare samples with different morphology these two parameters must be considered. A possible way of doing that is by dividing the FIAP or the IRF by the specific surface (m^2g^{-1}) of the sample. This normalisation has

also disadvantages. The surface area is a parameter difficult to know or even estimate. The cracks, fractures, gap and grain boundaries, makes it difficult to know the initial surface area. Moreover as the experimental time goes by, the dissolution produces changes in the surface that are very difficult to anticipate [14]. Being aware of this problematic, the normalisation using the specific surface is still a useful tool to compare fuel samples with different morphology.

In Table 12 the IRF of the different radionuclides at the end of the experiment is shown normalised by the specific surface (IRFS).

Table 12: IRF values at the end of the experiments normalised by the specific surface (IRFS).

IRFS (%) g m^{-2}	Rb	Sr	Cs
42BWR Segment	417±144	179±82	849±190
42BWR CORE	20±23	16±17	53±40
42BWR OUT	21±19	15±14	36±30
54BWR Segment	373±237	278±51	2631±466
54BWR CORE	23±35	34±37	62±38
54BWR OUT	25±17	15±28	31±17

4.3. Comparison between cladded segment and powder fraction experiments

It is possible to see a significant difference between the IRFS of the cladded segment and the IRFS of the powder fractions, especially for caesium. This difference persists even if the radionuclides dissolved during the washings are taken into account in the powder fraction experiments. The IRFS coming from the gap, fractures and cracks may be the responsible of this difference. During the irradiation of the fuel, the temperature in the centre of the pellet is higher than the periphery due to the effect of the coolant. Depending on its volatility and reactivity, the RN migrate towards the borders of the pellet where they get trapped and precipitate when the temperature decreases. Therefore, the gap between the pellet and the cladding is very rich in IRF RN as can be observed in this study. In addition, the inter-pellet space could be also very rich in IRF RN, but in this study the cladded segments were cut avoiding this gap in order to study only the effect of the gap between the pellet and the cladding. Further experiments are foreseen to study the effect of the space

between pellets. In the cladded segment the difference in the normalised IRF between radionuclides is higher than for the powder segments. This effect could be explained due to the differences in volatility and reactivity of the different elements that will affect its capacity to migrate through the fuel pellet.

4.4. Comparison between elements of cladded segment experiments

In the cladded segments the release of caesium is higher than the release of rubidium and higher than the release of strontium. It has to be taken into account that strontium should be dissolved in the UO_2 matrix due to its very low oxygen potential and even if strontium reaches its solubility limit and segregates into the grey phases, those phases are not volatile [15]. During the irradiation, if the temperature is high enough, both rubidium and caesium are in gas phase and therefore are more mobile than strontium, and reach the gap of the segment. The difference between the release of caesium and rubidium could be due to its diffusivity characteristics and chemical interactions.

4.5. Comparison between elements of powder fractions experiments

In the powder fraction experiments the release of caesium, rubidium and strontium is similar. In these experiments the IRF contribution comes from the grain boundaries where both caesium, rubidium and strontium seem to be segregated equally. It looks like the release of the CORE fraction is slightly higher than the release of the OUT fraction perhaps due to the protective effect of the HBS [1,7] but nevertheless the difference between fractions is very low.

4.6. Comparison between fuels

The experimental data was compared between the different fuels taking into account their irradiation history and morphological characteristics.

When comparing the fuels, it is possible to observe that the release is similar in all cases, powder and segment, with the exception of Cs in the cladded segment.

Our group collaborated with the European project FIRST Nuclides[16]. One of the conclusions of this project was the determination of a trend between LPD and FGR or IRF. Fuels with higher LPD also present higher FGR and IRF. Therefore the release of Caesium was expected to be higher for the 42BWR fuel due to its higher LPD. The LPD for the 42 BWR fuel is high, despite of its lower burnup and also the diameter is higher (9.4 mm) as compared to this of the 54BWR fuel (8.7 mm). Looking at the morphology of the fuel, the grain size was 15.0±1.0 for the 42BWR and 10.1±1.0 for the 54BWR.

It is known that a higher grain size implies a lower release. Consequently despite of having the higher LDP of the 42BWR fuel, its higher diameter and higher grain size could be the responsibles for its lower Cs release. In this case the effect of the grain size and the pellet diameter in the caesium release is higher than the effect produced by the LPD. It has to be remarked that the release of Cs in the cladded segment is higher in the 54BWR fuel, both looking at table 11 (IRF) and table 12 (IRFS), which means that the uncertainties of the surface area doesn't play any role in this case. Indeed, the FGR was also lower for the 42BWR fuel, coinciding with the release of Cs, despite having the higher LPD. Consequently, the reported sample related Cs IRF results are also valid for the pin related FGR values, excluding local artefacts.

It seems that an increase in the grain size and in the pellet diameter corresponds to a decrease in the release of a highly mobile radionuclide like caesium but doesn't affect much the release of less mobile radionuclides such as rubidium and strontium.

The results of this work were compared with data from experiments at similar conditions found in the literature [10, 17-20]. The comparisons for Cs, Rb and Sr are shown in the Figures 14, 15 and 16.

A previous work using a BWR fuel with similar irradiation conditions was performed by the same group [10]. In this case the fuel (53BWR) had a burn-up of 53GWd(t_{HM})$^{-1}$, a linear power density of 191 Wcm^{-1}, a fission gas release of 3.9 %, grain size of 16.0±1.0, a diameter of 8.7mm and was irradiated during 1370 days. The IRFS for Rb, Sr and Cs of the 53BWR fuel was similar for the powder fractions but one order of magnitude higher for the cladded segments. However it has to be taken into account that the 42BWR and 54BWR cladded segments were cut in the middle of a pellet, avoiding the space between pellets. This interpellet space may contain a high concentration of IRF radionuclides that could increase the IRF results. Indeed, in the gamma measurements of the whole pin, it is possible to determine the position of each dishing thanks to the accumulation of Cs. The 53BWR cladded segment was much bigger than the ones used in this work and contained the dishing. Therefore the high IRFS results of the 53BWR may be due to the presence of the dishing in the cladded segment experiment of this fuel. The difference in weight between the 53BWR and the fuels of this work should be reasonably corrected when normalising by the specific surface.

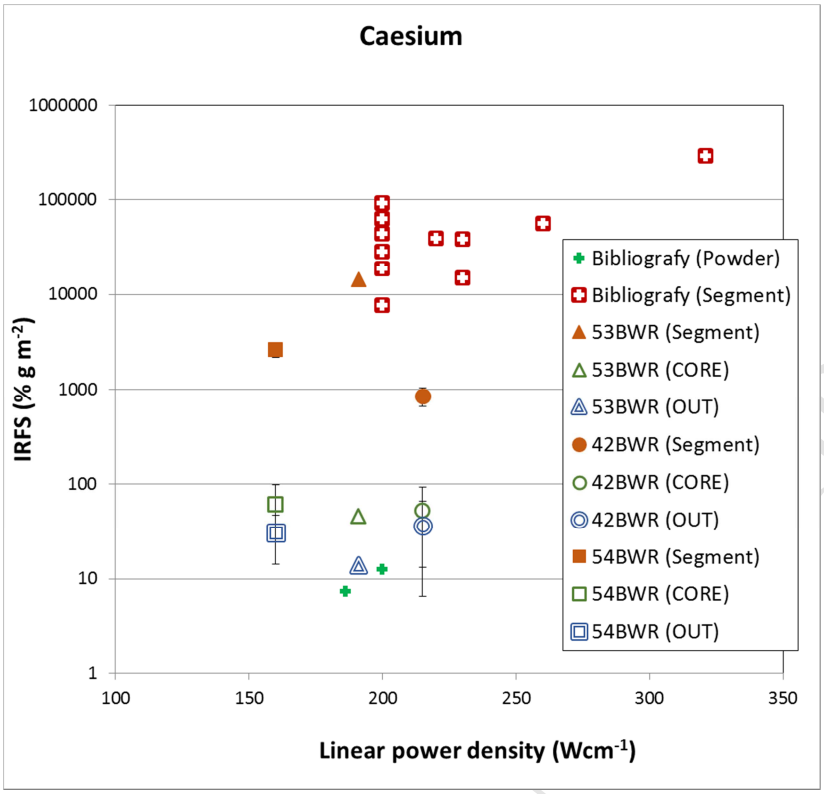

Figure 14: *IRFS (%gm^{-2}) vs. Linear power density (Wcm^{-1}) for caesium* [10, 17-20].

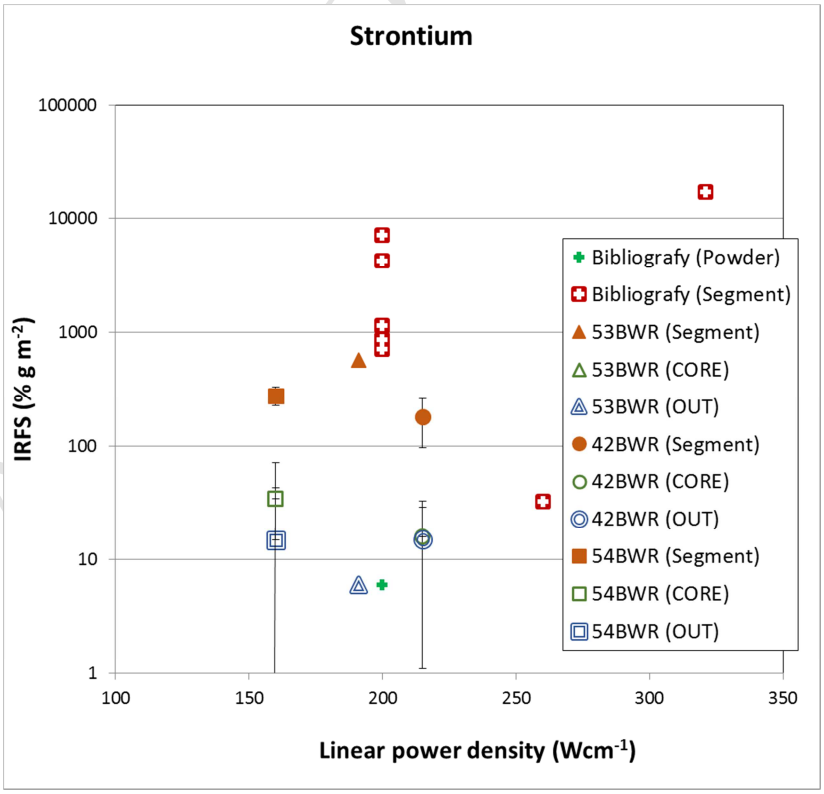

Figure 15: *IRFS (%gm^{-2}) vs. Linear power density (Wcm^{-1}) for strontium* [10, 17-20].

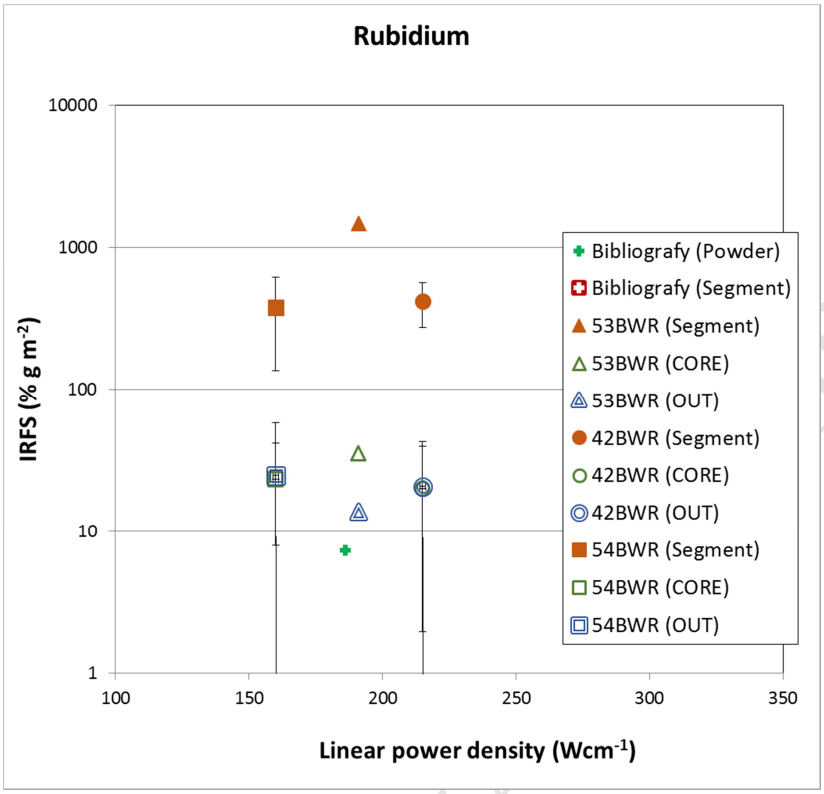

Figure 16: *IRFS (%gm^{-2}) vs. Linear power density (Wcm^{-1}) for rubidium* [10, 17-20].

The results obtained are slightly lower than the ones found in the literature for spent UO_2 fuels using carbonated solutions and similar experimental conditions [10, 17-20]. As discussed before, the effect of the interpellet space contribution on the total release could have played an important role, considering that all the segments found in the bibliography were cut including at least one dishing. More experiments need to be done in order to determine the effect of the dishing in the cladded segment samples since the lack of this interpellet space in the samples of this work could explain the lower release.

As expected, powder results presented lower IRFS due to the lack of the gap contribution and possible RN loses during the sample preparation.

5. Conclusions

Corrosion experiments were performed with two different BWR fuels. From each fuel three different regions were studied, a cladded segment without the interpellet space, powder from the centre of the pellet and powder from the periphery of the pellet. The outcome of these experiments was interpreted and reported in this paper.

In all the experiments Cs presented the highest release. Cs, Rb and Sr had a faster dissolution than the matrix in the experiments and can be considered as IRF. In the powder experiments, an initial IRF was observed for Mo and Tc but lasted only some days.

It was also observed a higher release of radionuclides during the first hours of the experiment followed by a slower release during the rest of the days. The higher release from the beginning is assumed to be due to the release coming from the void spaces: the gap and the cracks in the case of the segment and from the grain boundaries initially available to water corrosion in the case of the powder specimens. The second IRF contribution is attributed to the internal grain boundaries not initially accessible to the water.

IRF normalised to the specific surface (IRFS) shows different results for the powder fractions and cladded segment experiments. The IRFS of the radionuclides is higher in the cladded segment than in the powder fractions experiments due to the effect of the gap and possible loses during the powder preparation. The IRFS of caesium, rubidium and strontium in the powder fractions is similar. However in the cladded segment, due to the effect of the segregation to the gap, the IRFS of caesium is higher than the IRFS of rubidium and the IRFS of rubidium is also higher than the IRFS of strontium.

Although recent studies have shown a relationship between LPD and IRF [16], this work has demonstrated that other parameters such as the grain size, the pellet diameter and maybe the presence of the gap between pellets can have a sigfnicative influence in this relationship. More studies are foreseen to understand the effect of each parameter in the IRF, in order to be able to estimate the IRF of a UOx fuel from its irradiation history and morphological characteristics.

The data obtained in this work has been compared and found to be consistent with previous results found in the literature.

Acknowledgements

The research leading to these results has received funding from ENRESA Under ENRESA/ITU/CTM 31698 Agreement, the TECNIOSPRING fellowship programme from ACCIÓ and the European Union's European Atomic Energy Community's (Euratom) Seventh Framework Programme FP7/2007-2011 under grant agreement n° 295722 (FIRST-Nuclides project). The authors would also like to thank the work performed in this project by the technical staff of JRC-ITU.

References

1. D. Serrano-Purroy, F. Clarens, E. González-Robles, J.P. Glatz, D.H. Wegen, J. de Pablo, I. Casas, J. Giménez, A. Martínez-Esparza, Instant release fraction and matrix release of high burn-up UO_2 spent nuclear fuel: Effect of high burn-up structure and leaching solution composition, J. Nucl. Mater. 427 (2012) 249-258, http://dx.doi.org/10.1016/j.jnucmat.2012.04.036.
2. J.P. Hiernaut, T. Wiss, J.Y. Colle, H. Thiele, C.T. Walker, W. Goll, R.J.M. Konings, Fission product release and microstructure changes during laboratory annealing of a very high burn-up fuel specimen, J. Nucl. Mater. 377 (2008) 313-324, http://dx.doi.org/10.1016/j.jnucmat.2008.03.006.
3. P. Fors, P. Carbol, S. Van Winckel, K. Spahiu, Corrosion of high burn-up structured UO_2 fuel in presence of dissolved H_2, J. Nucl. Mater. 394 (2009) 1-8, http://dx.doi.org/10.1016/j.jnucmat.2009.07.004.
4. Y.H. Koo, B.H. Lee, J.S. Cheon, D.S. Sohn, Pore pressure and swelling in the rim region of LWR high burnup UO_2 fuel, J. Nucl. Mater. 295 (2001) 213-220, http://dx.doi.org/10.1016/S0022-3115(01)00535-9.
5. K. Lassmann, C.T. Walker, J. Van de Laar, F. Lindström, Modelling the high burnup UO_2 structure in LWR fuel, J. Nucl. Mater. 226 (1995) 1-8, http://dx.doi.org/10.1016/0022-3115(95)00116-6.
6. J. Spino, K. Vennix, M. Coquerelle, Detailed characterisation of the rim microstructure in PWR fuels in the burn-up range 40-67 GWd/tM, J. Nucl. Mater. 231 (1996) 179-190, http://dx.doi.org/10.1016/0022-3115(96)00374-1.
7. D. Serrano-Purroy, I. Casas, E. González-Robles, J.P. Glatz, D.H. Wegen, F. Clarens, J. Giménez, J. de Pablo, A. Martínez-Esparza, Dynamic leaching studies of 48 MWd/kgU UO_2

commercial spent nuclear fuel under oxic conditions, J. Nucl. Mater. 434 (2013) 451-460, http://dx.doi.org/10.1016/j.jnucmat.2011.03.020.

8. E. González-Robles, Study of radionuclides release in commercial UO_2 spent nuclear fuels, PhD. Thesis, Universitat Politècnica de Catalunya, Barcelona, 2011.

9. D. Serrano-Purroy, F. Clarens, J.-P. Glatz, D. Wegen, B. Christiansen, J. de Pablo, I. Casas, A. Martínez-Esparza, Leaching of 53 MW/d kg U spent nuclear fuel in a flow-through reactor, Radiochim. Acta 97 (2009) 491-496, http://dx.doi.org/10.1524/ract.2009.1640.

10. E. Gonzalez-Robles, D. Serrano-Purroy, R. Sureda, I. Casas, J. de Pablo, Dissolution experiments of commercial PWR (52 MWd/kgU) and BWR (53 MWd/kgU) spent nuclear fuel cladded segments in bicarbonate water under oxidizing conditions. Experimental determination of matrix and instant release fraction, Journal of Nuclear Materials 465 (2015) 63-70, http://dx.doi.org/10.1016/j.jnucmat.2015.05.012 .

11. FIRST NUCLIDES PROJECT. Fast / Instant Release of Safety Relevant Radionuclides from Spent Nuclear Fuel. Collaborative Project funded by the European Commission under the 7th Framework Programme of the European Atomic Energy Community (EURATOM) for research activities in support of implementation of geological disposal (Fission-2011-1.1.1).

12. E. Iglesias, J. Quiñones, Analogous materials for studying spent nuclear fuel: The influence of particle size distribution on the specific surface area of irradiated nuclear fuel, App. Surf. Sci. 254 (2008) 6890-6896, http://dx.doi.org/10.1016/j.apsusc.2008.04.091.

13. F. Clarens, J. de Pablo, I. Casas, J. Giménez, M. Rovira, Surface sites densities of uranium oxides: UO_2, U_3O_8. Mater. Res. Soc. Symp. Proc. 807 (2004) 71–76, http://dx.doi.org/10.1557/PROC-807-71.

14. B.D. Hanson, R.B. Stout. Re-examining the Dissolution of Spent Fuel: A Comparison of Different Methods for Calculating Rates, Mater. Res. Soc. Symp. Proc. 824 (2004) 89-94, http://dx.doi.org/10.1557/PROC-824-CC2.4.

15. H. Kleykamp. The chemical state of the fission products in oxide fuels, Journal of Nuclear Materials 131 (1985) 221-246, http://dx.doi.org/10.1016/0022-3115(85)90460-X.

16. K. Lemmens, E. González-Robles, B. Kienzler, E. Curti, D. Serrano-Purroy, R. Sureda, A. Martínez-Torrents, O. Roth, E. Slonszki, T. Mennecart, I. Günther-Leopold, Z. Hózer, J. Nucl. Mater. Submitted (2016).

17. D. Roudil, C. Jégou, V. Broudic, B. Muzeau, S. Peuget, X. Deschanels, Gap and grain boundaries inventories from pressurized water reactor spent fuels, Journal of Nuclear Materials 362 (2007) 411–415, http://dx.doi.org/10.1016/j.jnucmat.2007.01.086.

18. O. Roth, C. Askeljung, A. Puranen, M. Granfors, D. Cui, J. Low, Leaching of high burn up spent fuel with and without matrix dopants, Proceedings of Final Workshop FIRST-Nuclides and Spent Fuel Workshop 2014, Karlsruhe, (2014).

19. T. Mennecart, K. Lemmens, C. Cachoir, Characterisation and leaching tests for the experimental determination of IRF radionuclides from belgian high-burnup spent nuclear fuel, Proceedings of Final Workshop FIRST-Nuclides and Spent Fuel Workshop 2014, Karlsruhe, (2014).

20. L. Johnson, I. Günther-Leopold, J. Kobler Waldis, H.P. Linder, J. Low, D. Cui, E. Ekeroth, K. Spahiu, L.Z. Evins, Rapid aqueous release of fission products from high burn-up LWR fuel: Experimental results and correlations with fission gas release, J. Nucl. Mater. 420 (2012) 54-62, http://dx.doi.org/10.1016/j.jnucmat.2011.09.007.